Optics and Lasers in Engineering 117 (2019) 21–28

Contents lists available at ScienceDirect

Optics and Lasers in Engineering

journal homepage: www.elsevier.com/locate/optlaseng

Probing greenhouse gases in turbulent atmosphere by long-range open-path wavelength modulation spectroscopy

Jinbao Xia[a,d], Feng Zhu[a,b], Sasa Zhang[a,d,*], Alexandre Kolomenskii[a,*], Jian Dong[a], Kunihiro Okada[e], James Strohaber[c], Hans. A. Schuessler[a,f]

[a] Department of Physics and Astronomy, Texas A&M University, College Station, TX 77843-4242, USA
[b] School of Physics and Astronomy, Sun Yat-sen University, Zhuhai, Guangdong 519082, China
[c] Department of Physics, Florida A&M University, Tallahassee, Florida 323073, USA
[d] School of Information Science and Engineering, Shandong University, Jinan 25006, China
[e] Department of Physics, Sophia University, Tokyo, 1028554, Japan
[f] Science Program, Texas A&M University at Qatar, Doha 23874, Qatar

ARTICLE INFO

Keywords:
Wavelength modulation spectroscopy
Long open-path detection
Greenhouse gases monitoring

ABSTRACT

Open-path measurements of greenhouse gases yield valuable data for atmospheric research. We present such a method based on wavelength modulation spectroscopy to measure greenhouse gases. A movable platform was developed capable of detecting atmospheric variations of the concentrations of methane and carbon dioxide. The system was calibrated in the laboratory and then moved to the field for continuous automated measurements over paths of up to 2.6 km. The intensity modulation caused by turbulence was also measured. The continuous monitoring of methane was carried out for more than 30 h. Similar measurements of carbon dioxide were performed for about 10 h. The results show that the detection limits of methane and carbon dioxide are ~2 ppb and ~20 ppm with integration times of 60 s and 20 s, respectively. We conclude by discussing the achieved parameters in comparison to results obtained with other techniques, which shows that the developed sensor is a promising tool for monitoring of greenhouse gases.

1. Introduction

Global warming is an increasing environmental concern. To a large extend it is attributed to two most important anthropogenic greenhouse gases (GHG): carbon dioxide (CO_2) and methane (CH_4), which are the main drivers of climate warming, accounting for ~60% and ~16% of radiative forcing, respectively [1]. In situ measurements of GHG concentrations are valuable in developing warming models [2] and understanding the consequences of human activities [3–4]. We note that traditional point sensors can detect methane [5,6] and carbon dioxide [7,8] down to ppb and ppm concentrations, respectively. Such point sensors can form a global network for accessing the long term global trends. However, these point sensors may not adequately represent the mean concentrations of greenhouse gases over large areas. Open-path measurements provide the averaged values of the concentration in extended areas and effectively characterize the emissions and sinks of greenhouse gases, yielding the necessary data for transport modelling of the atmosphere.

Open-path measurements are based on the Beer-Lambert law and use a light source (laser or lamp) to measure the absorption spectrum on a given propagation path and retrieve the concentration of trace gases. Traditional open-path instruments based on Fourier transform spectroscopy (FTS) in the mid-IR [9,10] and differential optical absorption spectroscopy (DOAS) in the ultraviolet (UV) and visible [11,12] have been used for many years. The above mentioned FTS approach has the drawback of the optical path limitation to about hundred meters determined by the low brightness of conventional non-coherent light sources and the difficulty to collimate the beam over long distances. In addition, the measurement time of the FTS is determined by the full scan of the moving stage and thus cannot be very short. Although Griffith et al. recently measured greenhouse gases over 1.5 km by the near-IR FTS using 25 W broadband tungsten-quartz-halogen light source [13], the accurate measurements were hindered by the interference of stray radiation and limited acquisition time (84 scans over 5 min, corresponding to the acquisition time of ~3.6 s for one measurement).

The novel technique of dual frequency comb spectroscopy using two femtosecond fiber lasers with suitably chosen repetition rate differences [14,15] could overcome some drawbacks of the FTS. It enabled adaptive compensation of the decoherence from atmospheric turbulence as well as the detection of greenhouse gases across a ~2 km air path, achieving precision of ~0.86 ppm for CO_2 [15] and ~2.3 ppb for CH_4 with a ~2.2 km air path and ~5 min integration time, and has been used for

* Corresponding authors.
E-mail addresses: sasazhang@sdu.edu.cn (S. Zhang), a-kolomenski@physics.tamu.edu (A. Kolomenskii).

https://doi.org/10.1016/j.optlaseng.2019.01.008
Received 30 November 2018; Received in revised form 16 January 2019; Accepted 19 January 2019
Available online 5 February 2019

the detection of methane leaks in the field [16]. The interferogram for a single spectrum can be acquired in few milliseconds, which effectively decreases the influence of intensity modulation on the experimental data caused by atmospheric turbulence. Although dual frequency comb spectroscopy enables broadband and fast measurements, it requires expensive laser equipment and data acquisition electronics.

In this paper we report in situ open-path measurements of greenhouse gases over kilometer lengths with calibrated wavelength modulation spectroscopy (WMS). WMS is a simple and efficient technique to improve the signal-to-noise ratio. It was employed previously mainly for point detection of different trace gases: NH_3 in environmental research [17,18], for analysis of carbon monoxide isotopes in breath [19], for measuring atmospheric pollutants in environmental monitoring [20–22] and in combustion research [23]. Until now, the only report on an open-path long-range measurement by WMS was published by Michel et al. [24]. They used a quantum cascade laser with the output at ~8 μm wavelength and an optical power of 40 mW to measure methane over hundred meters. Despite larger absorption cross sections in the MIR, for measurements at longer distances the NIR can be a better choice because of weaker interference of water absorption and readily available emitting and receiving equipment developed for applications at telecommunication wavelengths.

We realized an automated operation and high sensitivity sensor enabling measurements over kilometers in open-path. In the setup, we used a narrow band laser source with ~2 nm tuning range and a narrow band optical filter to effectively reduce the stray radiation interference. A WMS reference channel was used to assess the effects of the atmospheric turbulence and for wavelength comparison. We calibrated the sensor by indoor measurements at different distances and carried out the field experiment at the Texas A&M University (TAMU) RELLIS campus. For the first time greenhouse gases were measured with WMS over such long distances (~1.3 km to the back-reflector and ~2.6 km for the round trip) in the near-IR. We also observed the effects of the atmospheric turbulence. Then, we tested the performance of the sensor and achieved a sensitivity of ~20 ppb with the integration time of 60 s for methane and of 20 ppm for carbon dioxide, integrating the signal over 20 s.

2. Detection principle and experimental setup

Modulation spectroscopy provides an effective way to achieve a high signal-to-noise-ratio. After modulating the laser current with the combination of a low frequency ramp and a high frequency sine voltage and passing the laser beam through a gas sample, the absorption information can be obtained by demodulating the received on the photodetector signal with a lock-in amplifier. In addition, to suppress the effect of the laser intensity variations due to scanning and different random factors, in our approach the 2*f*-signal was normalized to the 1*f*-signal, as was implemented successfully in Ref. [25].

In more details the WMS detection is described below. We assume that the incident laser intensity $I(t)$ and frequency $\nu(t)$ are temporarily modulated,

$$I(t) = I_0 + \Delta I \cos(\omega t) = I_0(1 + i_1 \cos(\omega t)) \tag{1}$$

$$\nu(t) = \bar{\nu} + \Delta \nu \cos(\omega t + \psi). \tag{2}$$

Here, I_0 is the average laser intensity, depending on the injected current, $i_1 = (\Delta I / I_0)$ is the modulation parameter, $\omega = 2\pi f$, where f is the modulation frequency, ν is the average frequency of the laser, $\Delta\nu$ is the frequency modulation amplitude, ψ is the phase shift between the intensity modulation and frequency modulation.

The transmission through the sample, $\tau(\nu)$ determined by a weak absorption of species *X,* can be expanded in a series of different harmonics as follows:

$$\tau(\nu) = \exp[-\xi X \varphi(\upsilon)] \approx 1 - \xi X \varphi(\upsilon) = 1 - \xi X \cdot \sum_{k=0}^{\infty} H_k \cdot \cos(k\theta) \tag{3}$$

where $\xi = pS_{ab}L_{op}$, $S_{ab} = S_{ab}(p,T)$ is the absorption line intensity depending on the pressure, p and temperature, T of the gas molecules, L_{op} is the optical path, $\varphi(\nu)$ is the absorption line profile, X is the concentration of the species of interest, $\theta = \omega t$ and the laser frequency ν is changing with scanning across the absorption line. The coefficients H_k (k is the harmonic index) can be expressed as

$$H_0 = \frac{1}{2\pi} \int_{-\pi}^{\pi} \phi(\nu) \cdot d\theta \tag{4}$$

$$H_k = \frac{1}{\pi} \int_{-\pi}^{\pi} \varphi(\nu) \cdot \cos(k\theta) d\theta, \quad k = 1, 2, 3.... \tag{5}$$

After demodulation with the lock-in detection unit, the first and second harmonic signals can be presented in the form [26]

$$s_{1f} \approx \frac{G\bar{I}_0}{2} i_1 \tag{6}$$

$$s_{2f} \approx -\frac{G\bar{I}_0}{2} \xi X H_2 \tag{7}$$

Here, G is the gain index of the photodetector. By dividing Eq. (7) by Eq. (6), we get the ratio S_s of the two harmonic signals:

$$S_s = \frac{s_{2f}}{s_{1f}} \approx -\frac{PS_{ab}L_{op}XH_2}{i_1}. \tag{8}$$

In the experiment two channels were used, one is the reference channel, yielding the ratio of harmonic signals S_R and the other is the measurement channel, yielding the ratio of harmonic signals S_M. The ratio of the signals from the two channels is calculated as

$$R_s = \frac{S_M}{S_R} = \frac{p_M s_M L_M X_M}{p_R s_R L_R X_R} = Z \cdot \frac{X_M}{X_R}, \tag{9}$$

where p_M, p_R are the pressures, s_M and s_R are the absorption line intensities, $L_M = 2L$ (L is the distance from the laser source to the retroreflector) and L_R are the optical paths and X_M and X_R are the unknown and known concentrations of the species of interest for the measurement and reference channels, respectively. Z is the known parameter, which was calculated using the values of pressure and temperature,

$$Z = \frac{s_M p_M L_M}{s_R p_R L_R}. \tag{10}$$

With Eq. (10) the unknown concentration X_M can be determined using the measurement results.

The schematic of the open path optical system is shown in Fig. 1. Two single-mode continuous commercial Distributed Feedback Diode Lasers (DFB-DL) with a fiber tail were selected as the laser sources with the wavelengths ~1654 nm and ~1602 nm (corresponding to the absorption features of methane and carbon dioxide, respectively) and the output powers of 10 mW each. The laser driver in the experiment is a commercial laser diode controller (ILX Lightwave, LDC-3724) with high stability and low noise current, combined with a thermoelectric temperature controller. The output from the DFB-DL laser was split into two beams by 99/1 fiber optic splitter (Thorlabs). The first beam (with ~99% of the transmitted power) after collimation was overlapped on a dichroic beam splitter (Thorlabs, DMSP650) with a CW green laser beam with a power of 20 mW, which was used for the optical path alignment. Then the overlapped beams passed a home-made beam expander, consisting of two lenses with focal lengths $f = 25$ mm and $f = 150$ mm, and went over a 1.3 km path in the air to the retroreflector array with the total area 95 cm^2, which was composed of three same size hollow retroreflectors of 65 mm diameter. The reflected light was collected by a telescope, filtered by a bandpass filter with a 10 nm spectral width and focused by a lens with $f = 200$ mm on an InGaAs Avalanche Photodetector (APD). The other beam (with ~1% of the transmitted power) went through a gas cell with calibrated methane or carbon dioxide gas with concentrations of 1% and 100%, respectively, and was focused onto an InGaAs PD by a lens. The two signals were acquired by a 16 bit, multifunction I/O

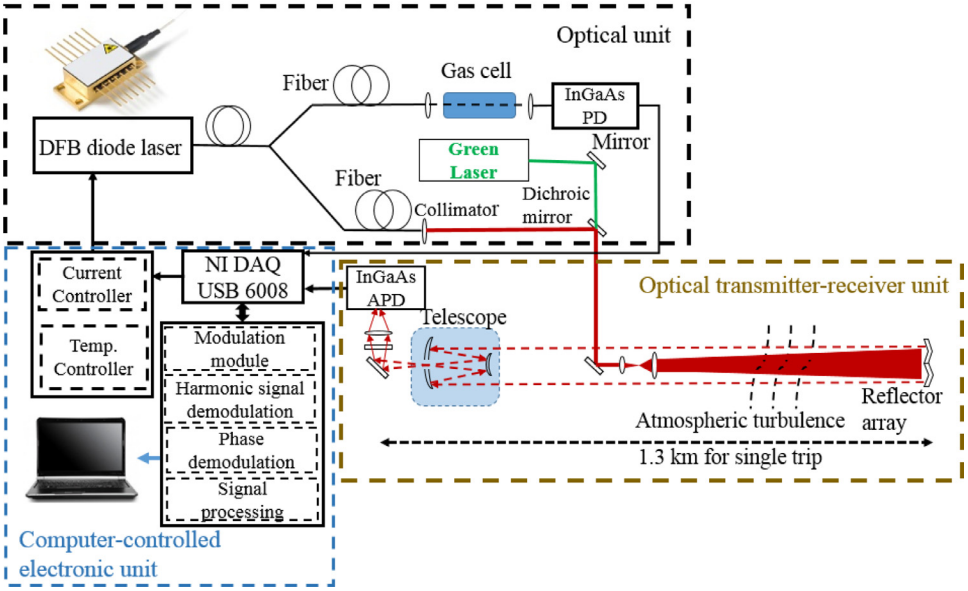

Fig. 1. Schematic of the long open-path optical sensing system.

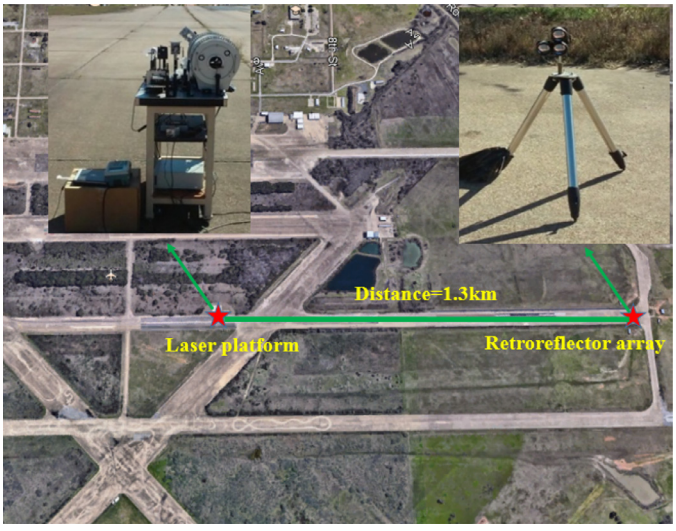

Fig. 2. The aerial view of the 1.3 km measurement path at the TAMU RELLIS Campus along one of the aircraft runways. The laser platform (shown in the left inset) was on a movable cart, the retroreflector (the right inset) was mounted on a tripod standing at the end of the runway.

device (National Instruments, USB6361) having 16 analog inputs and two analog outputs and further processed.

An updated LabVIEW program based on our previous work [27] was used for the system control and spectral measurements. The software has the functions of the laser scanning and modulation, data acquisition, harmonic signal demodulation, phase demodulation and saving the data.

The platform was tested in the hall of the laboratory building and then moved to the TAMU RELLIS campus airport. The laser platform was located in the middle of the runway (30° 38′06.41″ N, 96° 28′54.06″ W) and the associated retroreflector was located at the end of the runway (30° 37′ 24.61″ N, 96° 28′ 53.92″ W). The path location is illustrated in Fig. 2. The elevations of the laser platform and retroreflector were 77.7 m and 78.1 m. The distance measured with a laser rangefinder was 1.306 km with precision of ±1 m. Insets in Fig. 2 show the mobile platform and retroreflector array.

The portability was assured by the sensor design and a power supply from 3600 Watt portable generator (BlackMax) with an outlet of 120 V, 30 A which kept the sensor continuously running about 10 h without interruption. The meteorological parameters in the field were recorded by home-made and calibrated pressure and temperature sensors. The data were digitized in real time by a DAQ card (National Instruments, USB6008) with a 100 Hz sampling rate and averaged over 1 s.

3. Experimental results

3.1. Indoor measurements

To assess the sensitivity and the distance dependence of the normalized signal due to methane absorption at the 1654 nm absorption band, the performance of the sensor was first tested in the basement hallway of the TAMU Mitchel Physics building. Backscattering of the laser light from a white paper attached to a board mounted on the tripod was received by the telescope and focused on the photodiode, providing sufficient signal. The tripod was positioned at seven different distances of 7.5, 12.5, 17.5, 22.5, 27.5, 32.5, and 37.5 m, respectively. The temperature, air pressure and humidity in the basement, which were 73.7F, 1.01 kPa and 51%, respectively, were almost constant and monitored by the sensors.

For each distance the normalized methane signal was integrated for ten minutes and the data were plotted as a function of the distance (Fig. 3). The dependence can be well fitted by the linear relation $\text{Signal}=8.09\times10^{-4}+7.97\times10^{-4}\times(\text{distance})$ with the R-square value of 0.986. The methane concentration in the building basement was measured to be 2.1 ± 0.1 ppm.

3.2. Outdoor measurements

The transmission of the laser beam through the atmospheric air besides the air flow turbulence is affected by absorbing gaseous components and atmospheric aerosols, which result in variations of the amplitude and phase of the received backscattered laser light. Consequently, the observed signal fluctuations reflect the influence of all these random factors. The fluctuations become more pronounced with increasing distance. Consequently, in measurements of methane in ambient air over a kilometer or longer optical paths, the fluctuations of the signal should be taken into account. Traditionally, the atmospheric turbulence is measured by a stellar scintillometer or LIDAR [28]. Tao Wei et al. [29]

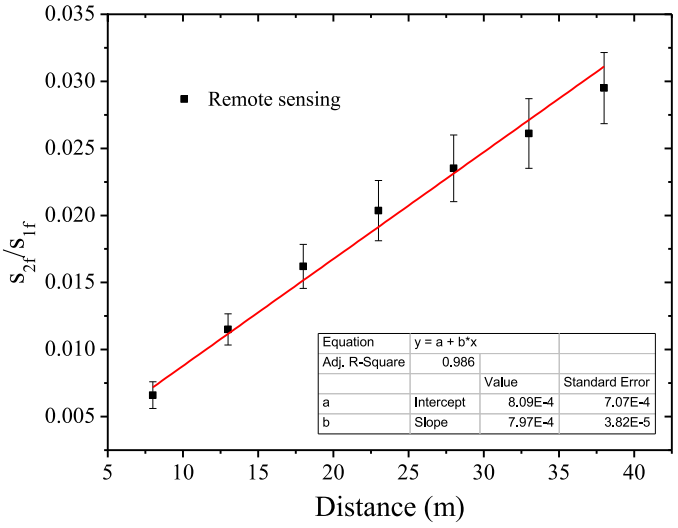

Fig. 3. The dependence of the calibrated methane signal on the distance with a linear fit.

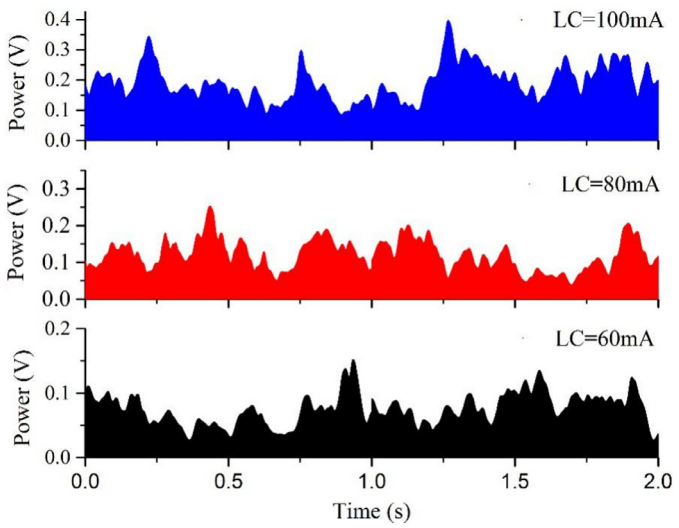

Fig. 4. The power data over ~2.6 km path acquired for different laser currents (LC).

developed a simple double pass turbulence monitoring system with a 5 MW peak power laser pulse source, using a corner retroreflector for improving the system sensitivity. Compared to the pulsed laser monitoring system, our low power continuous near infrared system (10 mW) avoids development of nonlinear propagation effects. The retroreflector array allowed our system to perform measurements over the distance to the retroreflector of up to 1.3 km. In this respect, the developed platform worked not only as a gas sensor, but also as a double-pass turbulence monitoring system.

In the experiment, we used the laser power from the reference channel to assess the stability of the received laser power from the measurement channel. The turbulence intensity can be directly characterized by the degree of the signal instability, i.e. the transmission of the laser radiation through the atmosphere can monitor the atmospheric turbulence and be further analyzed statistically. For the continuous double pass system, the scintillation index, $\sigma^2(\vec{r}, L_M)$, describing the variations of the light power transmitted through the atmosphere, is defined as a function of the log-irradiance variance [29] or the linear variance [30].

Here, we use the linear variance

$$\sigma^2(\vec{r}, L_M) = \left\langle (\delta S)^2 \right\rangle, \tag{11}$$

where $\langle\rangle$ is the averaging operator over a set of measurements, $\delta S = \Delta s/\bar{s}$ characterizes relative variations (instability) of the signal; $\Delta s \propto (P - \bar{P})$ and $\bar{s} \propto \bar{P}$ represent the deviation and average value of the signal related to the instantaneous (P) and average ($\bar{P}$) values of the intercepted radiation power. For the conditions of weak turbulence, the Rytov variance of the turbulence effect on the propagating beam is given by

$$V(L_M) = 1.23 C_n^2 {k_L}^{7/6} {L_M}^{11/6}, \tag{12}$$

where C_n^2 is the refractive index structure parameter, used to characterize the effects of atmospheric turbulence, $k_L = 2\pi/\lambda$ is the wavenumber of the laser, and L_M is the optical path. In our setup, the round trip distance was used in Eq. (10). In the weak fluctuation regime ($\sigma^2(\vec{r}, L_M) < 1$) the scintillation index should be equal to the Rytov variance [30],

$$\sigma^2(\vec{r}, L_M) = V(L_M). \tag{13}$$

Then from this equation, the C_n^2 parameter can be estimated.

In the experiment, the laser temperature was controlled to be 15 °C with precision of 0.001 °C. The frequency variation for the fixed laser frequency is less than 100 MHz, and in different measurements the laser current was set to fixed values of 60 mA, 80 mA and 100 mA,

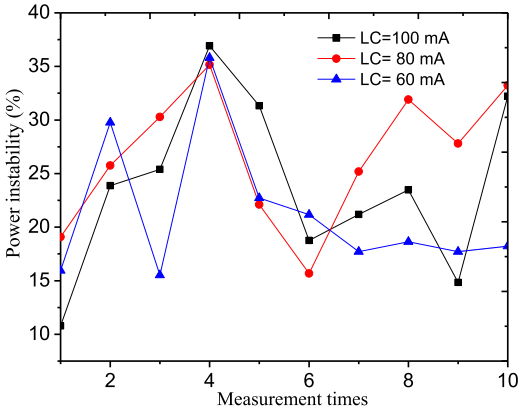

Fig. 5. The instability of the received laser power due to turbulence effects for different laser currents.

which correspond to the laser wavelength of 1604.21 nm, 1604.28 nm and 1604.45 nm. The data was acquired for 2 s by the DAQ card with acquisition rate of 400 kHz, thus providing 800k points. The acquired signal is depicted in Fig. 4. It is obvious that the received power experiences sharp fluctuations resulting from turbulence. The mean signal values from the detector were 0.075 V, 0.119 V and 0.019 V for the three different laser currents, and the standard deviation values were 0.025 V, 0.042 V and 0.06 V, respectively.

To further analyze the instability of the received power, the data was divided into 10 groups, each group having 80k points equal to the acquisition time of 0.2 s. For each group the average signal of the measured laser power, $\bar{s}$, and the RMS-deviation, Δs, and the signal instability $\delta S = \Delta s/\bar{s}$ (shown in Fig. 5) were calculated. For different laser currents, the power varied from 10% to 35%, showing that the choice of the laser current could not mitigate the power instability, thus, occurring due to the turbulence effects. From the plots of Fig. 5 using Eqs. (11,12) the refractive index structure parameter C_n^2 was calculated; at different laser currents close values were obtained: $C_n^2 = 9.6 \times 10^{-15} m^{-2/3}$ for the laser current (LC) 100 mA, $C_n^2 = 9.7 \times 10^{-15} m^{-2/3}$ for LC=80 mA and $C_n^2 = 9.5 \times 10^{-15} m^{-2/3}$ for LC=60 mA, showing consistency of these results.

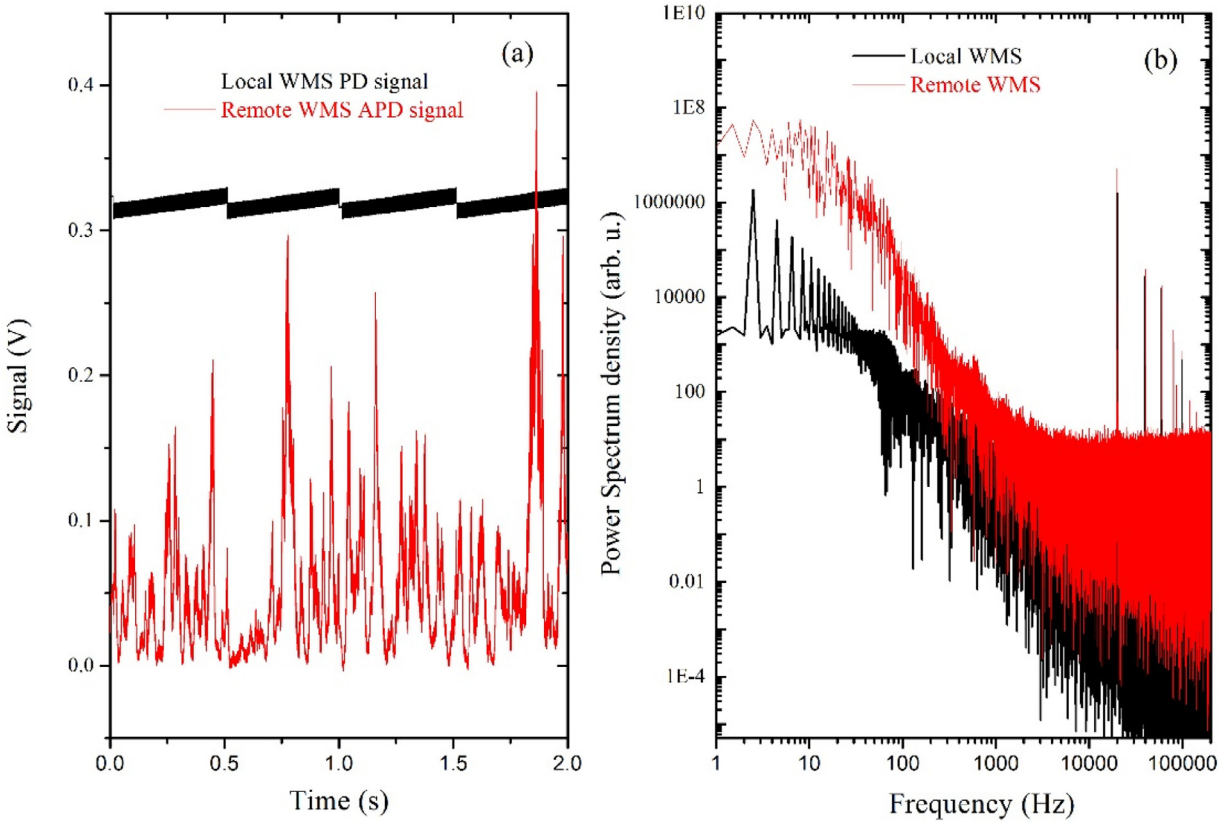

Fig. 6. Signals from photodetectors for the reference channel (black line) and remote sensing channel (red line): (a) the measured signals, (b) the power spectral densities.

3.3. Methane and carbon dioxide measurements

To make it easier to catch the back-reflected near-IR light on the photodiode, we utilized a 20 mW visible green laser as a guide to coarsely adjust the height of the retroreflector array. Then, the fine adjustments were carried out to maximize the back-reflected near IR signal. We used a cell with a standard concentration of 1% of methane in the reference channel. The ramp voltage amplitude was varied from 6 V to 8 V, corresponding to the injected current from 60 mA to 80 mA. The scan and modulation frequencies were 2 Hz and 20 KHz, respectively. The ramp and sine waves were generated by the LabVIEW software with the sampling rate of 400 kHz. A fourth-order Butterworth low pass filter with the cut-off frequency of 9 Hz was set in the digital lock-in amplifier. The initial signals from the reference and remote sensing channels were recorded as shown in Fig. 6. In Fig. 6(a); the red line is the modulated signal from the beam that passed through the turbulent atmosphere. The black line is the modulated signal from the local reference photodetector. As can be seen, the reference signal is stable, while the remote sensing signal is strongly fluctuating due to turbulence.

The power spectral densities (PSDs) of the two signals were obtained by the conversion from the time domain to the frequency domain, as shown in Fig. 6(b). In Fig. 6, the black line shows the higher harmonic frequencies in the PSD of the local reference signal with the ramp frequency 2 Hz and the modulation frequency 20 kHz. It is worth noting that the remote sensing signal (red line), although not clearly exhibiting the harmonics of the ramp frequency, still shows the higher harmonics of the modulation frequency.

The demodulated first and second harmonic signals are shown in Fig. 7. After demodulation and averaging the signals exhibit only a minor influence of the atmospheric turbulence, showing that the WMS signal is rather robust. The amplitude of the *2f*-signal normalized to the 1*f*-signal was used for the determination of the concentration according to Eq. (8). The observed small time shift between the center of the reference signal and the measurement signal is mainly due to their different processing delays.

The measurements were recorded from 23:00, October 4th to 7:00 October 6th of 2017 for 32 h of total data, as weather and field available time permitted. The mean pressure was 1.012 atm, with instantaneous values changing from 1.008 atm to 1.106 atm, i.e. within 4.9% of the relative amplitude variation (see Fig. 8). The temperature showed the highest value of 28 °C and the lowest temperature of 22 °C with relative amplitude variations within 12%. The results for methane were averaged every 60 s and presented in Fig. 9, showing that the measured methane concentration varied between 2 ppm and 3.5 ppm. These values are mostly larger than the commonly accepted average atmospheric value (~2 ppm) due to other methane sources within nearby farming areas. There were several intervals with different behavior: around 24:00 on October 4th there were several oscillations observed followed by a slowly changing methane concentration till ~9:00 am, October 5th and then on the same date again several oscillations from 2.4 ppm to 3.2 ppm were observed. Since there was some traffic on the runway, the sharp spikes in the interval enclosed in the dashed rectangle are due to the laser beam interruptions by passing cars. Then again an interval with small variations follows until the methane concentration increases showing a variation up to 3.0 ppm at ~7:00, October 6th again.

The sensor precision was evaluated by the Allen variance analysis of the measurement over 1000s (Fig. 10). It was about 100 ppb with the integration time of 1 s and down to 20 ppb with integration of 60 s, which confirms that the variations induced by noise were low enough, thus enabling the accurate monitoring of the methane concentration.

For measurements of the carbon dioxide in the atmospheric air we replaced the DFB laser to have the center wavelength at the CO_2 absorption band of 1602 nm and used the reference cell filled with 100% carbon dioxide. The settings of the parameters were the same as before.

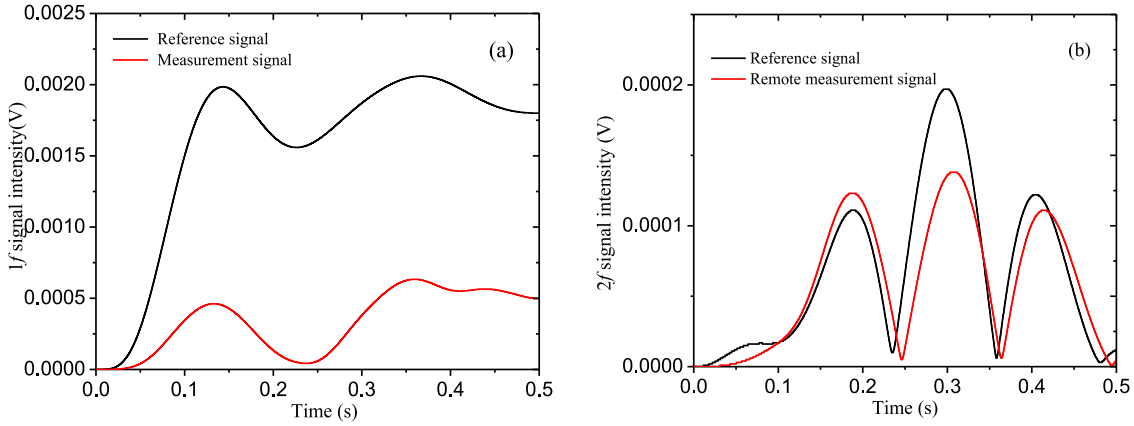

Fig. 7. Demodulated signals from the reference channel (black line) and the remote measurement channel (red line): (a) the first harmonic and (b) the second harmonic.

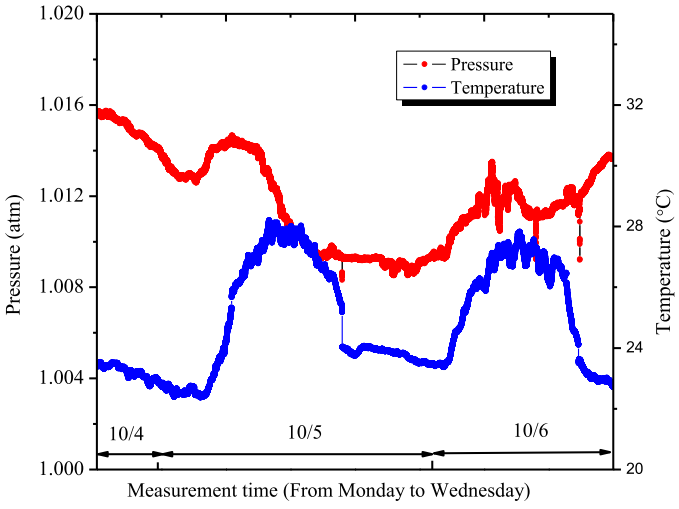

Fig. 8. The measured pressure and temperature during measurements on October 4–6, 2017.

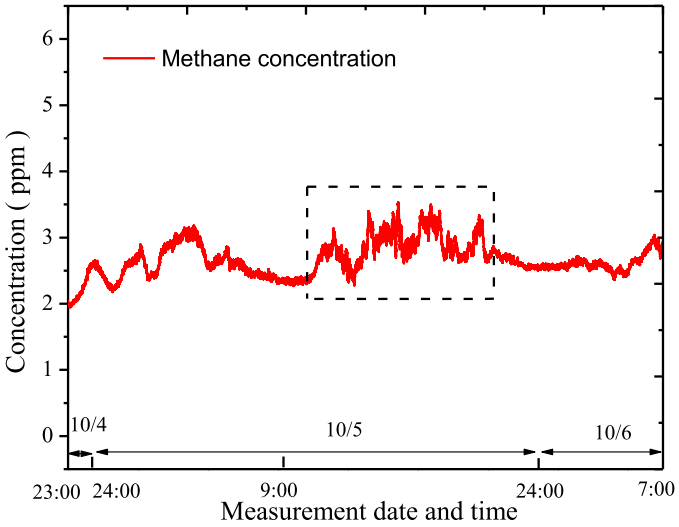

Fig. 9. The measured methane concentration for October 4–6, 2017. The observed sharp spikes on 10/5 (data within the dashed rectangle) were caused by the interruptions of the laser beam by passing cars. Larger scale variations observed on 10/4, 10/5 and 10/6 reflect the variations of the methane concentration due to the local agricultural and livestock activities.

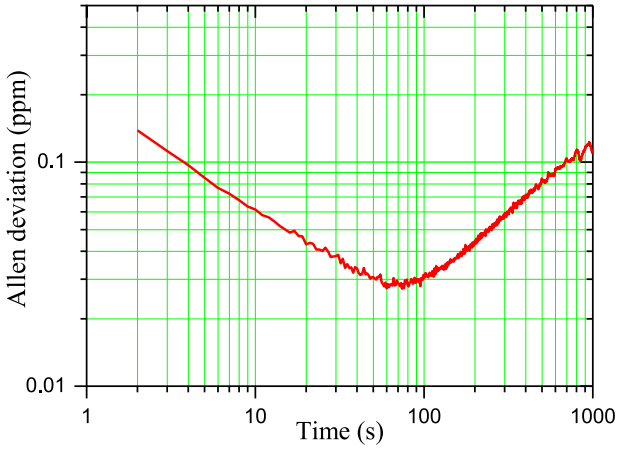

Fig. 10. The Allen variance analysis of the precision of the sensor for methane, showing the optimal integration time of ~60 s.

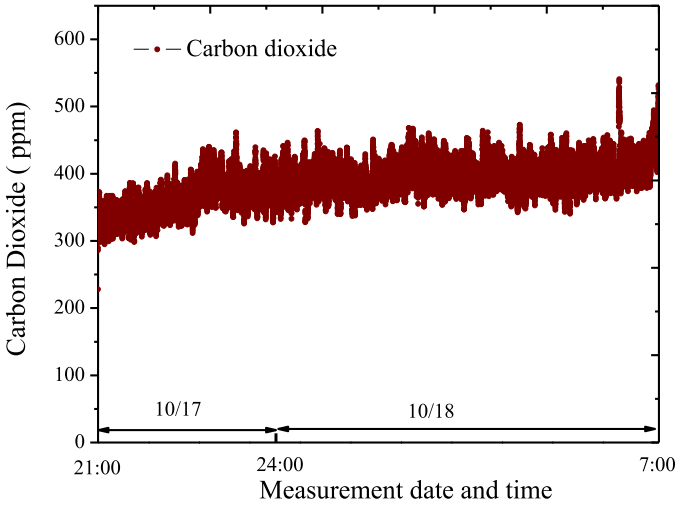

Fig. 11. The measured behavior of the carbon dioxide concentration (on 10/18 and 10/19 of 2017).

The modulation amplitude was changed to 1 V due to the linewidth difference between the carbon dioxide and methane. We recorded the carbon dioxide normalized WMS signal for 10 h, as shown in Fig. 11 after conversion of the results to the concentration values. The concentration

Table 1
Comparison of long-path techniques for detection of CH_4 and CO_2 in the near-IR spectral region.

Techniques	Laser source	Distance (round trip)	Allan dev. CH_4 (ppb)	Allan dev. CO_2 (ppm)	Turbulence measurement	Reference
WMS	DFB (12 mW)	2.6km	20 @1 min	30 @20s	Yes	This work
FTS	Lamp (35 W)	1.5 km	12 @5min	1.6 @5min	No	[13]
DCS	Fiber laser (-)	2 km	<5 @5min	<1 @ 5min	Yes	[15]
DOAS	Broadband source (200 mW)	5.1km	–	–	No	[12]

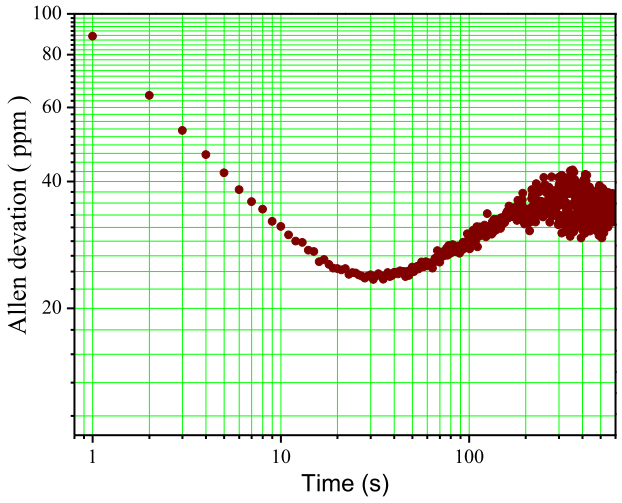

Fig. 12. The Allen variance analysis of the precision of the sensor for carbon dioxide.

of carbon dioxide was about 400 ppm and remained almost constant, showing smaller relative variations compared to methane. To evaluate the detection limit, the Allan variance over 600 s was also calculated as depicted in Fig. 12. The achieved precision was about 20 ppm with integration time of 20 s. The sensitivity of the sensor to carbon dioxide was not as good as for methane. Partially, this is due to the stronger wind on the day of the carbon dioxide experiment compared to the conditions for the methane experiment.

So far only four techniques (our technique included) for greenhouse gases over kilometer-long paths were reported. The results for these four different measuring platforms are summarized in Table 1. We characterized these techniques from four aspects: (1) the laser source (with the power shown), (2) optical path length, (3) Allan deviation for CO_2 and CH_4, and (4) whether turbulence measurements were performed. The work we present here, although using lower laser power, shows comparable performance for methane detection. For carbon dioxide the sensitivity of our sensor is somewhat lower than with the other techniques, which is accounted for by the lower ramp frequencies, lower laser power and unfavorable weather conditions. In the future, we will do more work on increasing the ramp frequencies and signal filtering to improve the detection limit of the system and make the system even more compact.

4. Conclusions

In this paper, we explored the greenhouse gas detection over long distances (up to 2.6 km) by a mobile sensor in the near infrared spectral region on the basis of the wavelength modulation spectroscopy technique. We used this sensor, first, to analyze the stability of the back-reflected laser power produced by the turbulence. Then the automated measurements of methane and carbon dioxide were performed for many hours. The sensitivities of the sensor for methane and carbon dioxide were evaluated to be 20 ppb and 20 ppm at the integration times of 60 s and 20 s, respectively. The sensor sensitivity can be improved by increasing the ramp frequency to reduce the turbulence influence. Although being rather compact and simple, our instrument has shown the sensitivity for methane detection comparable to more complex instruments, such as DCS. The developed sensor provides the possibility for monitoring of greenhouse gases (CH_4 and CO_2). It can also be used as a leak detector for methane gas in the oil/gas industry.

Acknowledgments

This work was supported by the National Key Basic Research Program of China(2015CB921003), the Robert A. Welch Foundation, grant No. A1546, and the Qatar Foundation, grant NPRP 8-735-1-154

References

[1] Butler JH, Montzka SA. The NOAA annual greenhouse gas index (AGGI). Updated: Spring; 2018. www.esrl.noaa.gov/gmd/aggi/aggi.html.
[2] Cox PM, Betts RA, Jones CD, Spall SA, Totterdell IJ. Acceleration of global warming due to carbon-cycle feedbacks in a coupled climate model. Nature 2000;408:184–7.
[3] Shindell DT, Miller RL, Schmidt GA, Pandolfo L. Simulation of recent northern winter climate trends by greenhouse-gas forcing. Nature 1999;399:452–5.
[4] Santer BD, Painter JF, Bonfils C, Mears CA, Solomon S, Wigley TML, Gleckler PJ, Schmidt GA, Doutriaux C, Gillett NP, Taylor KE, Thorne PW, Wentz FJ. Human influences on atmospheric temperature. Proc Natl Acad Sci 2013;110:17235–40.
[5] Liu K, Wang L, Tan T, Wang G, Zhang W, Chen W, Gao X. Highly sensitive detection of methane by near-infrared laser absorption spectroscopy using a compact dense–pattern multipass cell. Sensor Actuat B: Chem 2015;220:1000–5.
[6] Nikodem M, Krzempek K, Dudzik G, Abramski K. Hollow core fiber-assisted absorption spectroscopy of methane at 3.4 um. Opt Express 2018;26:21843–8.
[7] Lewicki R, Wysocki G, Kosterev AA, Tittel FK. Carbon dioxide and ammonia detection using 2 μm diode laser based quartz-enhanced photoacoustic spectroscopy. Appl Phys B 2007;87:157–62.
[8] Wang Z, Wang Q, Ching JY-L, Wu JC-Y, Zhang G, Ren W. A portable low-power QEPAS-based CO2 isotope sensor using a fiber-coupled interband cascade laser. Sensor Actuat B: Chem 2017;246:710–15.
[9] You Y, Staebler RM, Moussa SG, Su Y, Munoz T, Stroud C, Zhang J, Moran MD. Long-path measurements of pollutants and micrometeorology over Highway 401 in Toronto. Atmos Chem Phys 2017;17:14119–43.
[10] Richter D, Erdelyi M, Curl RF, Tittel FK, Oppenheimer C, Duffell HJ, Burton M. Field measurements of volcanic gases using tunable diode laser based mid-infrared and Fourier transform infrared spectrometers. Opt Lasers Eng 2012;37:171–86.
[11] Somekawa T, Manago N, Kuze H, Fujita M. Differential optical absorption spectroscopy measurement of CO_2 using a nanosecond white light continuum. Opt Lett 2011;36:4782–4.
[12] Platt U, Perner D. Measurements of atmospheric trace gases by long path differential UV/visible absorption spectroscopy. Opt Laser Remote Sens 1983:97–105.
[13] Griffith DWT, Pöhler D, Schmitt S, Hammer S, Vardag SN, Platt U. Long open-path measurements of greenhouse gases in air using near-infrared Fourier transform spectroscopy. Atmos Meas Tech 2018;11:1549–63.
[14] Rieker GB, Giorgetta FR, Swann WC, Kofler J, Zolot AM, Sinclair LC, Baumann E, Cromer C, Petron G, Sweeney C, Tans PP, Coddington I, Newbury NR. Frequency–comb-based remote sensing of greenhouse gases over kilometer air paths. Optica 2014;5:290–8.
[15] Giorgetta FR, Rieker GB, Baumann E, Swann WC, Sinclair LC, Kofler J, Coddington I, Newbury NR. Broadband phase spectroscopy over turbulent air paths. Phys Rev Lett 2015;115:103901–4.
[16] Coburn S, Alden C, Wright R, Cossel K, Baumann E, Truong G, Giorgetta F, Sweeney C, Newbury N, Prasad K, Coddington I, Rieker G. Regional trace-gas source attribution using a field-deployed dual frequency comb spectrometer. Optica 2018;5:320–7.
[17] Besson JP, Schilt S, Rochat E, Thevenaz L. Ammonia trace measurements at ppb level based on near-IR photoacoustic spectroscopy. Appl Phys B 2006;85:323–8.
[18] Miller DJ, Sun K, Tao L, Khan MA, Zondlo MA. Open-path, quantum cascade-laser-based sensor for high-resolution atmospheric ammonia measurements. Atmos Meas Tech 2014;7:81–93.
[19] Ghorbani R, Schmidt FM. ICL-based TDLAS sensor for real-time breath gas analysis of carbon monoxide isotopes. Opt Express 2017;25:12743–52.
[20] Tao L, Sun K, Amir Khan M, Miller DJ, Zondlo MA. Compact and portable open–path sensor for simultaneous measurements of atmospheric N 2 O and CO using a quantum cascade laser. Opt Express 2012;27:28106–18.

[21] Dong L, Yu Y, Li C, So S, Tittel FK. Ppb-level formaldehyde detection using a CW room-temperature interband cascade laser and a miniature dense pattern multipass gas cell. Opt Express 2015;13:19821–30.
[22] Stachowiak D, Jaworski P, Krzaczek P, Maj G, Nikodem M. "Laser-based monitoring of CH4, CO2, NH3, and H2S in animal farming—system characterization and initial demonstration. Sensors 2018;18:529.
[23] Tao B, Hu Z, Fan W, Wang S, Ye J, Zhang Z. Novel method for quantitative and real-time measurements on engine combustion at varying pressure based on the wavelength modulation spectroscopy. Opt Express 2017;25:762–76.
[24] Michel APM, Miller DJ, Sun K, Tao L, Stanton L, Zondlo MA. Long-path quantum cascade laser–based sensor for methane measurements. J Atmos Ocean Technol 2016;17:2373–84.
[25] Rieker GB, Jeffries JB, Hanson RK. Calibration-free wavelength-modulation spectroscopy for measurements of gas temperature and concentration in harsh environments. Appl. Optics 2009;29:5546–60.
[26] Peng Z, Ding Y, Chen L, Li X, Kangjie Z. Calibration-free wavelength modulated TDLAS under high absorbance conditions. Opt Express 2011;23:23104–10.
[27] Xia J, Zhu F, Zhang S, Kolomenskii A, Schuessler H. A ppb level sensitive sensor for atmospheric methane detection. Infrared Phys Technol 2017;86:194–201.
[28] Zhai X, Wu S, Liu B. Doppler lidar investigation of wind turbine wake characteristics and atmospheric turbulence under different surface roughness. Opt Express 2017;12:515–29.
[29] Wang T, Wang W, Du P, Geng D, Gao G, Gong M. Double-pass propagation of laser pulses reflected by a diffuse whiteboard or a corner-cube retroreflector in turbulent atmosphere. Opt Laser Eng 2014;55:94–8.
[30] Zhang M, Tang X, Lin B, Ghassemlooy Z, Wei Y. Analysis of Rytov Variance in Free Space Optical Communication under the Weak Turbulence. 2017 16th International Conference on Optical Communication and Networks; 2017.